Proceedings of the Canadian Society for Mechanical Engineering International Congress
32nd Annual Conference of the Computational Fluid Dynamics Society of Canada
Canadian Society of Rheology Symposium
CSME-CFDSC-CSR 2025
May 25–28, 2025, Montréal, Québec, Canada

UNSTEADY WAKE CHARACTERISTICS OF A NOTCHBACK AHMED BODY

Joseph K. Kodie-Ampaw[1*], Adime K Bonsi[1], Ebenezer E. Essel[1]
[1]Department of Mechanical, Industrial and Aerospace Engineering, Concordia University, Montreal, Canada
[*]joseph.kodieampaw@concordia.ca

Abstract — The unsteady wake dynamics of a notchback Ahmed body with an effective backlight angle of $\beta_e = 17.8°$ is investigated using time-resolved particle image velocimetry (TR-PIV). The study was conducted at a Reynolds number of $Re_h = 17{,}000$ based on the height h of the model and freestream velocity $U_e = 0.24\,m/s$. Velocity field measurements were conducted in two streamwise-wall-normal planes offset from the centerline, VL (left) and VR (right). The results showed an earlier attachment of the separated shear layer from the roof on the deck in VR than in VL, indicating wake asymmetry. Spectral proper orthogonal decomposition (SPOD) of the velocity fluctuations in the slant-deck region identified coherent structures with dominant Strouhal numbers of $St_h = 0.92$ in VL and $St_h = 0.89$ in VR. These structures are larger and more energetic over the slant and deck in VL compared to VR. In contrast, the structures on the roof were more prominent in VR, influencing the earlier attachment on the deck. The convective velocity of these structures further demonstrated asymmetry in the downstream evolution.

Keywords - Bluff bodies; notchback Ahmed body; flow separation; vortex shedding; coherent structures

I. INTRODUCTION

Ground vehicles account for approximately 75% of transportation-related greenhouse gas (GHG) emissions, significantly contributing to climate change [1]. Reducing these emissions through drag reduction techniques and vehicle electrification requires a comprehensive understanding of vehicle aerodynamics. This knowledge is essential for developing effective flow control strategies to minimize drag, which in turn reduces fuel consumption and increases the driving range of electric vehicles per charge. Furthermore, insights on vehicle aerodynamics improves fundamental understanding of complex turbulent flow phenomena such as flow separation, vortex shedding and multiple shear layer interactions around bluff bodies.

The aerodynamics of ground vehicles are often studied using simplified models such as the Ahmed body and Windsor body. The standard Ahmed body, first introduced by Ahmed et al. [2], is a hatchback model that simulates the wake characteristics of sport utility vehicles (SUVs) [2]. The model consists of a fore-end with rounded edges, a rectangular midsection, and a slanted rear-end with a vertical base. The salient flow features include a flow separation at the trailing edge of the roof which leads to the formation of separation bubble on the slanted surface. Subsequent separation at the top and bottom trailing edges of the vertical base generates counter-rotating recirculation bubbles, associated with strong downwash from the top and upwash from the gap between the body and the wall. Moreover, flow separation from the sides of the slant and their interaction with the flow over the slant generate a pair of counter-rotating longitudinal vortices, often referred to as C-pillar vortices. These complex three-dimensional (3D) vortex systems are further complicated when a trunk is attached to the vertical base, forming a notchback Ahmed body (Fig.1) that mimic sedans [3].

For the notchback, the separated flow from the roof may attach onto the deck of the trunk or shed directly into the wake behind the vertical base, depending on the backlight angle β and the effective backlight angle β_e [3], [4]. The backlight angle β is defined as the inclination angle of the slant, while β_e represents the angle formed by a straight line connecting the trailing edges of the roof and the deck (Fig.1).

Most of the previous studies on Ahmed bodies were conducted with the hatchback model or squareback model that represents the flatback of semi-trailers and buses [5]. As a result, our understanding of the wake dynamics of the notchback is relatively limited. Previous studies have shown that wake characteristics of the notchback depends on important parameters such as β, β_e [3], [4], Reynolds number based on

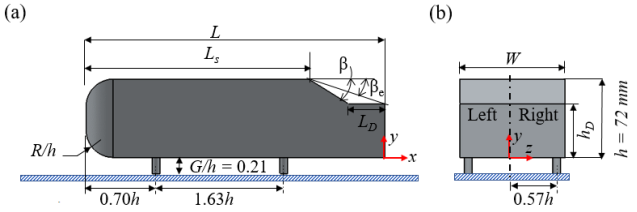

Figure 1. Schematic of the notchback Ahmed body with the nomenclature used.

the height (h) of the body and the freestream velocity (U_e) Re_h [6], and the geometry (sharp/roundness) of the roof trailing edge [6]. Sims-Williams et al. [3] investigated the effects of β ($17.8° - 90°$) and β_e ($17.8° - 31.8°$) angles on the wake structure of notchback configurations at $Re_h = 50000$. The experiments were conducted using surface flow visualization, particle image velocimetry (PIV) and were augmented by 3D numerical simulations using unsteady Reynolds-averaged Navier–Stokes (URANS). Two main flow regimes were identified based on β_e: reattached flow ($\beta_e < 25.3°$) on the deck and fully separated flow ($\beta_e \geq 25.3°$). Sims-Williams et al. [3] also found that within the reattached flow regime, the notchback geometries exhibit a symmetric wake topology at $\beta_e = 21.0°$ and an asymmetric wake topology at $\beta_e = 17.8°$. The asymmetric wake structure has also been observed in previous flow visualization studies of a notchback car by Cogotti [7].

He et al. [4] conducted large eddy simulation (LES) of the unsteady wake dynamics of the notchback at $\beta_e = 17.8°$ and $\beta_e = 21.0°$ based on the experiments of Sims-Williams et al. [3]. The asymmetric case ($\beta_e = 17.8°$) exhibited a stochastic wake bimodality with large timescales, similar to bimodality observed behind squareback models [8]. The asymmetry of the wake was attributed to asymmetric separation from the roof of the body and the associated asymmetric reattachment on the deck. He et al. [9] investigated the effects of blockage ratio, $BR \in [0, 20]$ on the bimodality of the notchback ($\beta_e = 17.8°$) and found that the wake becomes symmetric when $BR > 10$. In [6], rounding the trailing edge of the roof was also observed to suppress wake bimodality. He et al. [6] further examined the effects of high Re_h $(50000, 100000, 2500000)$ on the asymmetric state of the notchback $\beta_e = 17.8°$ using LES and wind tunnel experiments (pressure taps and hot wire measurements). At $Re_h = 50000$, the wake exhibited bimodality, but as the Reynolds number increased, it transitioned into a tri-stable state, due to the emergence of an additional symmetric wake state. He et. al [10] demonstrated that floor motion, mimicking on road conditions of vehicles has negligible impact on the degree of wake asymmetry. Recently, Ouedraogo and Essel [11] conducted an extensive numerical study on the effects of low-Reynolds number ($5000 < Re_h < 50000$) on a notchback $\beta_e = 17.8°$ using RANS. The results categorized the wake structure into symmetric ($Re_h < 10000$), transitional ($10000 < Re_h < 35000$), and fully asymmetric ($Re_h > 35000$) states, demonstrating the sensitivity of wake asymmetry to Reynolds number.

The objective of the present study is to investigate the unsteady wake dynamics of the notchback with $\beta_e = 17.8°$ using a time-resolved particle image velocimetry (TR-PIV). To the authors' knowledge, time-resolved experiments for the notchback with $\beta_e = 17.8°$ have not been published. Therefore, the present study not only enhances physical insight but also provides a benchmark dataset for validating future numerical simulations and models.

II. EXPERIMENTAL SETUP AND PROCEDURE

The experiments were conducted in an open recirculating water channel at the University of Manitoba. Fig 2 shows a schematic of the channel's test section with the Ahmed body installed on a false floor raised 50 mm above the floor of the channel. The transparent test section has dimensions of $6.00\ m \times 0.45\ m \times 0.60m$ in the streamwise, vertical and spanwise directions, respectively. The notchback model used is a 1:4 scaled down version of the original Ahmed body [2]. The model has height $h = 72\ mm$, $W = 1.35h$, $L = 3.82h$, $L_D = 0.469h$, $R = 0.347h$ and $h_D = 0.687h$ with support legs of diameter $0.1h$ (Fig 1). The false floor of length $42h$ spanned the entire width of the test section. To minimize flow separation, the leading and trailing edges of the plate are sharp-edged with a 45° angle [8]. The blockage ratio, defined as the ratio of the frontal area of the model to the cross-sectional area of the inlet of the test section, is 2.6%. The origin of the Cartesian coordinate is at the bottom trailing edge of the model with x, y and z in the streamwise, wall-normal and spanwise directions, respectively.

To investigate unsteady wake asymmetry of the notchback, TR-PIV measurements were conducted in two streamwise-wall-normal (x-y) planes offset from the centerline; i.e., $z/h = -0.417$ (left) and $z/h = 0.417$ (right), denoted as VL and VR, respectively, for brevity. The flow was seeded with $10\mu m$ silver-coated hollow glass spheres, with specific gravity of 1.4 and illuminated with a dual-head high-speed Nd: YAG laser ($30\ mJ/pulse, \lambda = 527\ nm$). The stokes number was below 0.05 ensuring the seeding particles follow the flow faithfully [12]. Two 12-bit CMOS cameras, each with a resolution of 2560×1600 pixels, were used to capture a wide flow field ($x/h \in [-3.83, 3.00], y/h \in [-0.21, 2.00]$). The two fields of view (FOVs) (Fig. 2) each have dimensions of $4h \times 2.5h$ with 15mm overlap. Based on a convergence test, a sample size of 60000 instantaneous images were acquired for each measurement plane at 806 Hz. Data were processed using DaVis version 10.0.5 software from LaVision Inc. The initial interrogation window was set to 128×128 pixels with a 50% overlap, and refined to a final interrogation window 24×24 pixels with a 75% overlap, allowing high spatial resolution. The uncertainty in the mean velocities less than 2% while the Reynolds stresses are about 10%.

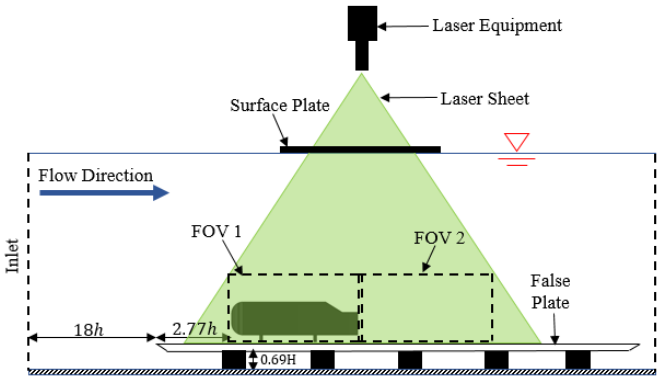

Figure 2. Schematic of the experimental setup and the field of views, FOVs (not to scale)

As summarized in Table 1, the upstream flow is a uniform flow with freestream velocity, $U_e = 0.24\ m/s$, corresponding to $Re_h = 17000$. The water temperature was maintained at $20°C$. The water depth D referenced from the test section floor

was $435mm$. The Froude number, $Fr = U_e/\sqrt{gD}$ where $g = 9.81ms^{-2}$ was 0.012, implying negligible free surface wave [13]. The freestream streamwise turbulence intensity T_u was 1.5%.

TABLE I. SUMMARY OF UPSTREAM APPROACH FLOW CONDITIONS

Re_h	U_e (m/s)	Tu (%)	Fr
17000	0.24	1.5	0.012

III. RESULTS AND DISCUSSION

A. Mean Flow and Turbulence Statistics

Fig. 3 shows the contours of the streamwise (U) and wall-normal (V) mean velocities in the VL ($z/h = -0.417$) and VR ($z/h = 0.417$) planes. The mean streamlines are superimposed on the velocity contours to reveal the flow pattern, while the isopleth of $U/U_e = 0$ is used to define the boundary of the reverse flow regions ($U/U_e < 0$). The wake structure exhibits a recirculation bubble on the slant and deck and a pair of recirculation bubbles behind the vertical base. However, the size of the bubble on the slant-deck region is larger in VL than in VR, demonstrating wake asymmetry, in agreement results of Ouedraogo and Essel [11] at a similar Reynolds number. The reattachment length on the deck, L_r (see Fig. 3(a)) is defined as the streamwise distance from the attachment point to the trailing edge of the deck, while the recirculation length L_R (Fig. 3(b)) is defined as the streamwise distance from the vertical base to

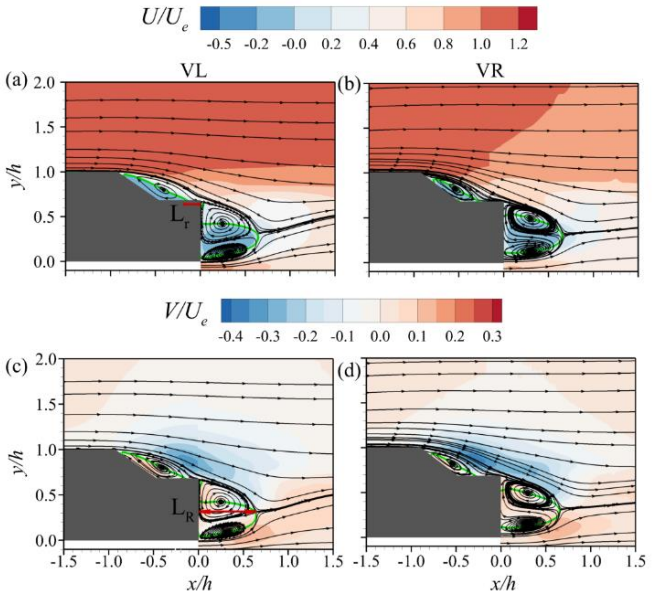

Figure 3. Contours of normalized (a, b) streamwise U and (c, d) wall normal mean velocity V, superimposed with mean streamlines in the streamwise planes VL (left) and VR (Right) . The green line represents the isopleth of $U/U_e = 0$. L_r and L_R labels represent reattachment and recirculation length respectively.

farthest extent of the reverse flow region behind the base. In VL, $L_r = 0.143$ but significantly increases to $L_r = 0.643$ in VR. Moreover, the recirculation lengths $L_R = 0.643$ in VL and $L_R = 0.670$ in VR. The values L_r and L_R in VL and VR indicate a larger degree of wake asymmetry over the slant and deck compared to the wake behind the vertical base of the body. The contours of the wall-normal mean velocity (V) demonstrated that the earlier attachment of the separated shear layer on the right side of the deck (VR) is due to a stronger downwash ($V < 0$) in VR than in VL, which is consistent with the results of Ouedraogo and Essel [11].

Fig. 4 compares the contours of the Reynolds stresses ($\overline{u'u'}$, $\overline{v'v'}$ and $\overline{u'v'}$) in the VL and VR planes. The results reveal three distinct shear layers: the separated shear layer from the roof, the second separated shear layer from the trailing edge of the deck after reattachment and the shear layer associated with the upwash flow at the bottom of the vertical base. The location and magnitude of the peak Reynolds stresses in the shear layer from the roof are comparable in both VL and VR planes. However, the Reynolds stresses in the upper shear layer behind the vertical base are significantly enhanced in VR compared to VL. The upwash shear layer, on other hand, depicts enhanced streamwise Reynolds normal stress and Reynolds shear stress in VL compared to VR. The streamwise location of the peak wall-normal Reynolds normal stress can be used to estimate the vortex formation length of the vortices shed in the shear layer of

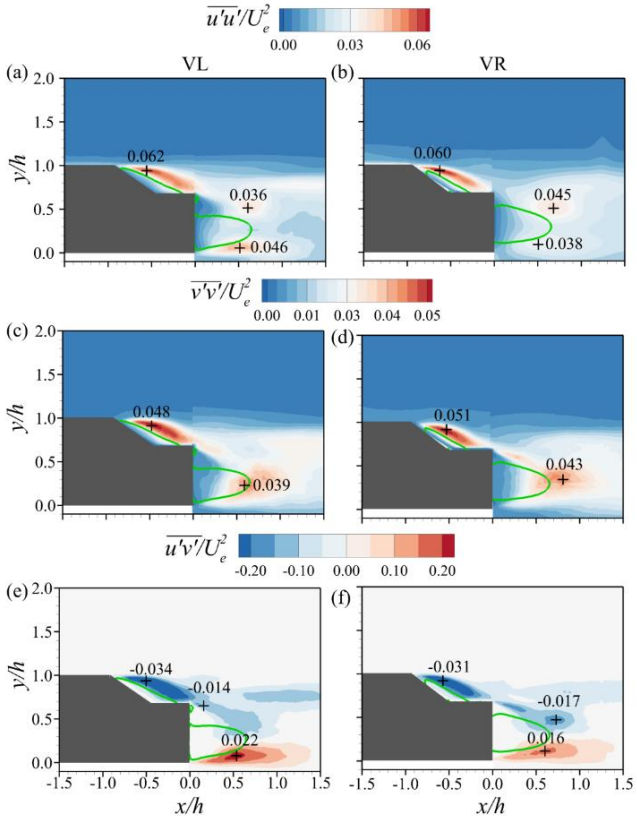

Figure 4. Contours of normalized Reynolds stresses (a, b) $\overline{u'u'}$ (c, d) $\overline{v'v'}$ and (e, f) $\overline{u'v'}$ in the streamwise planes VL (left) and VR (Right) . The green line represents the isopleth of $U/U_e = 0$.

the body. The vortex formation length, $l_f/h = 0.53$ and 0.81 in VL and VR, respectively, suggests that the asymmetric attachment of the separated shear layer on the deck results in a

Identify applicable sponsor/s here. *(sponsors)*

delay in wall-normal vortex shedding on the right side of the body compared to the left.

B. *Spectral Proper Orthorgonal Decomposition*

Proper orthogonal decomposition (POD) [14] and its variant, spectral POD (SPOD) [15], are robust techniques used to effectively extract energetic large-scale structures (coherent structures) in the flow field and investigate their dynamic roles in turbulence transport phenomena. POD decomposes the flow field into an orthogonal set of spatial modes ranked by energy level, with lower-order modes capturing the most energetic structures. On the other hand, SPOD sorts the spatial modes based on the convective velocities of the structures, providing an efficient approach to isolating dominant unsteady flow phenomena, such as vortex shedding. He et al. [4] used POD to investigate that the coherent structures in the asymmetric wake of a notchback with $\beta_e = 17.8°$, while Chen et al. [5] used SPOD to investigate bimodality and pumping motion (i.e., expansion and contraction) of the recirculation bubbles in the wake of a squareback Ahmed body.

In the present study, SPOD is used to examine the coherent structures associated with vortex shedding in the wake of the notchback body. The time-resolved velocity field was transformed into the frequency domain using Fourier transform, and at each frequency, a decomposition into orthogonal modes was performed using POD. Accordingly, the fluctuating velocity components is expressed as

$$\vartheta'(x,y,t) = \sum_{j=1}^{\infty}\sum_{m=1}^{\infty} \phi_j^m(x,y) a_j^m e^{-i\omega_j t} + \text{c.c.} \qquad (1)$$

where ϕ_j^m is the orthogonal set of spatial eigenfunctions (modes) and a_j^m their associated coefficients, and the wavenumber $\omega_j = 2\pi f_j$. The total sample of 60000 snapshots were used and divided into 10 batches. SPOD was performed within a masked region ($x/h \in [-1.40, 0], y/h \in [0.60, 1.70]$) over the slant and deck to examine the coherent structures associated with the asymmetric wake.

Fig. 5 presents the pre-multiplied energy spectra of the first five SPOD modes in both VL and VR planes. The Strouhal number is defined as $St_h = fh/U_e$. In each plane, the spectra shows multiple dominant St_h, demonstrating the complex interactions of several flow phenomena over the slant-deck region of the notchback. For example, Chen et al. [5] showed that behind a squareback model, $St_h < 0.014$, $St_h \in [0.014, 0.123]$, $St_h \in [0.123, 0.234]$ and $St_h \in [0.234, 1.024]$ are associated with bimodality, flapping motion of the wake, vortex shedding and shear layer instabilities, respectively. In the present study, the plot indicated that the peaks of the spectra are more pronounced in VL than in VR. Mode 1 shows that the dominant Strouhal number associated with vortex shedding over the slant is $St_h = 0.92$ in VL but marginally reduced to $St_h = 0.89$ in VR.

The fractional and cumulative energy distribution of the first 10 SPOD modes to the turbulent kinetic energy associated with structures responsible for vortex shedding, are presented in Fig. 6. In VL, Mode 1 accounts for 40% of the energy, but significantly reduced to 30% in VR. However, the fractional energy for Mode 2 is about 15% in both VL and VR. Fig. 6b demonstrates that fewer modes are required to reconstruct a reduced-order velocity field in VL compared to VR, indicating a wider range of scales and greater complexity in VR.

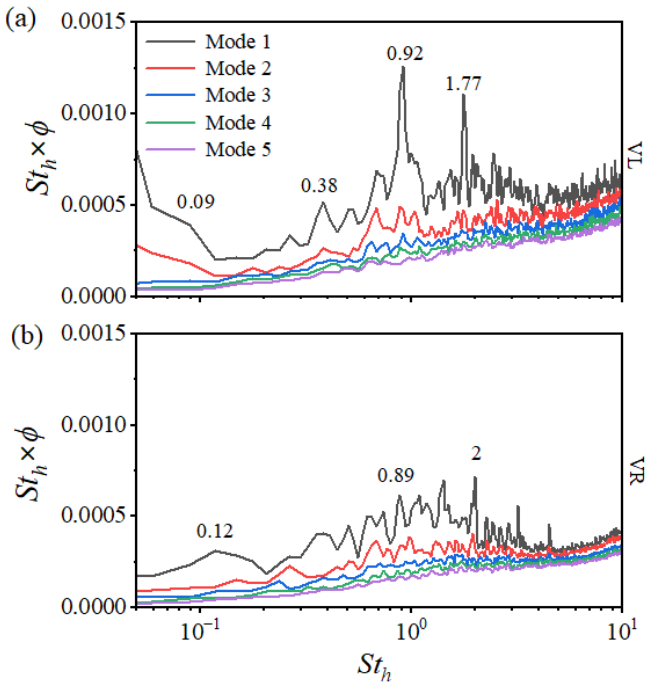

Figure 5. Pre-multiplied spectra of eigenvalues for the first five SPOD modes of the velocity field in the near wake, shown for (a) VL and (b) VR streamwise planes. The labels indicate the dominant strouhal numbers.

The spatial distributions of Mode 1 for dominant Strouhal numbers $St_h = 0.92$ (VL) and 0.89 (VR) are shown in Fig. 7. Fig. 7 (a) and (b) display the normalized streamwise component of the mode $\phi_u/\phi_{u,max}$, while Fig. 7 (c) and (d) show the normalized wall-normal component of the mode $\phi_v/\phi_{v,max}$. In both planes, coherent structures are observed in the separated shear layer from the roof and convected downstream into the wake region behind the vertical base. However, the structures are relatively larger and more intense in VL than in VR, consistent with the frequency spectra (Fig. 5) and the contours of $\overline{u'u'}$ and $\overline{u'v'}$. In contrast, it interesting to note that, the structures on the roof are larger and more intense in VR, suggesting that the asymmetry in the roof structures and subsequent separation at the trailing edge contribute to the asymmetric attachment on the deck. The convective velocity of the structures ($U_c = \Lambda f$) can be estimated based on the local wavelength ($\Lambda/2$), defined as the streamwise distance between peaks of alternating positive and negative structures [16]. Fig 7 (c) shows that, in VL, $\Lambda/2$ increases from $0.23h$ to $0.41h$ over the slant, corresponding to $U_c/U_e \in [0.42, 0.75]$. However, due to earlier attachment in VR, $\Lambda/2$ decreases from $0.23h$ ($U_c/U_e = 0.41$) to $0.20h$ ($U_c/U_e = 0.36$) near the trailing edge of the deck. In the wake behind the base, structures are more organized and convect with $U_c/U_e \in [0.68, 0.78]$ in VR.

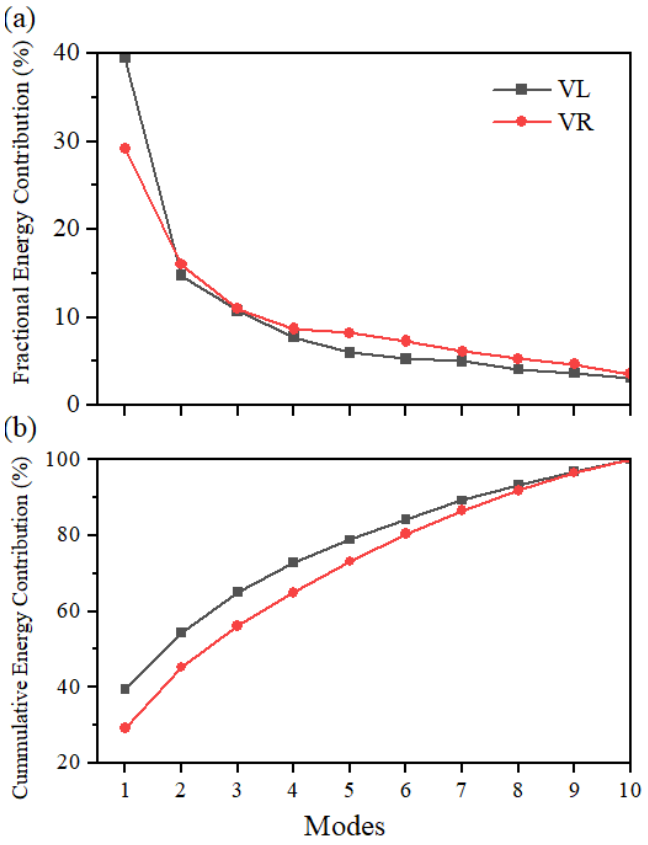

Figure 6. Distributions of the (a) fractional energy and (b) cumulative energy contributions of the first ten modes at similar dominant Strouhal numbers for (a) VL ($St_h = 0.92$) and (b) VR ($St_h = 0.89$) streamwise planes.

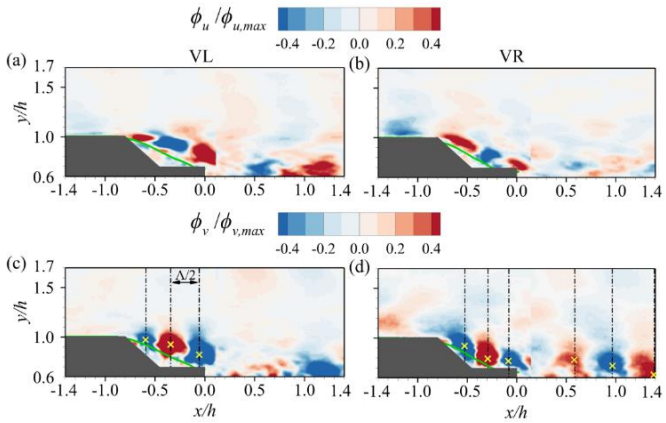

Figure 7. Contours of (a, b) streamwise and (c, d) wall-normal components of Mode 1 at the dominant Strouhal numbers ($St_h = 0.92$) in the left VL and right VR ($St_h = 0.89$).

IV. CONCLUSION

Time-resolved PIV was used to investigate the unsteady wake dynamics of the notchback Ahmed body with an effective backlight angle of $\beta_e = 17.8°$ at a Reynolds number, $Re_h = 17000$. Measurements were obtained in two streamwise-wall-normal planes (VL and VR) offset from the symmetry line at a sampling frequency of $806Hz$.

The mean flow showed a larger recirculation bubble over the slant-deck region in VL compared to VR, demonstrating wake asymmetry. A stronger downwash contributed to earlier attachment of the separated shear layer from the roof on the deck in VR. The differences in reattachment (L_r) and recirculation (L_R) lengths between the two planes indicated that the asymmetry was stronger over the slant and deck than behind the vertical base. The Reynolds stress distributions showed comparable peak locations and magnitude in the shear layers from the roof. However, the stresses were enhanced in the downwash behind the vertical base in VR, while the upwash shear layer exhibited stronger stresses in VL. The vortex formation length indicated that the asymmetric attachment of the separated shear layer on the deck caused a delay in wall-normal vortex shedding in the VR plane.

The SPOD highlighted the wake asymmetry in the notchback, with stronger spectral peaks and larger coherent structures in VL than in VR. The dominant Strouhal number associated with vortex shedding is slightly higher in VL ($St_h = 0.92$) than in VR ($St_h = 0.89$), and Mode 1 contributes more energy in VL (40%) compared to VR (30%). The spatial modes showed larger structures in the separated shear layer over the slant in VL, while the roof structures are more intense in VR, influencing the earlier attachment on the deck. In VR, the convective velocity of the structures reduced near the trailing edge of the deck, due to earlier shear layer attachment, and these structures were more organized in the wake behind the vertical base compared to the structures in VL.

ACKNOWLEDGMENT

The authors are grateful to the Natural Sciences and Engineering Research Council of Canada (NSERC) for their financial support through NSERC Discovery Grant for E.E.E. We are also grateful to Dr. Mark F. Tachie for granting access to the experimental facility at the University of Manitoba.

REFERENCES

[1] H. Ritchie, "Cars, planes, trains: where do CO_2 emissions from transport come from?," *Our World in Data*, 2020.

[2] S. R. Ahmed, G. Ramm, and G. Faltin, "Some salient features of the time-averaged ground vehicle wake," *SAE Transactions*, vol. 93, pp. 473–503, 1984, doi.org/10.4271/840300.

[3] D. Sims-Williams, D. Marwood, and A. Sprot, "Links between notchback geometry, aerodynamic drag, flow asymmetry, and unsteady wake structure," *SAE Int. J. Passenger Cars - Mech. Syst.*, vol. 4, no. 1, pp. 156–165, 2011, doi: 10.4271/2011-01-0166.

[4] K. He, G. Minelli, J. Wang, T. Dong, G. Gao, and S. Krajnović, "Numerical investigation of the wake bi-stability behind a notchback Ahmed body," *J. Fluid Mech.*, vol. 926, pp. 1–29, 2021, doi: 10.1017/jfm.2021.748.

[5] C. W. Chen, S. Wang, and S. Ghaemi, “Spectral proper orthogonal decomposition of time-resolved three-dimensional flow measurements in the turbulent wake of the Ahmed body,” *J. Fluid Mech.*, vol. 985, p. A19, 2024, doi: 10.1017/jfm.2024.288.

[6] K. He, G. Minelli, X. Su, G. Gao, and S. Krajnović, “Influence of the rounded rear edge on wake bi-stability of a notchback bluff body,” *Phys. Fluids*, vol. 33, no. 11, pp. 115107-1–115107-20, 2021, doi: 10.1063/5.0071925.

[7] A. Cogotti, “Car-wake imaging using a seven-hole probe,” *SAE Tech. Paper* 860218, pp. 1–12, 1986, doi: 10.4271/860218.

[8] M. Grandemange, M. Gohlke, and O. Cadot, “Bi-stability in the turbulent wake past parallelepiped bodies with various aspect ratios and wall effects,” *Phys. Fluids*, vol. 25, no. 9, p. 095103, 2013, doi: 10.1063/1.4820372.

[9] K. He, G. Minelli, X. Su, G. Gao, and S. Krajnović, “Blockage influence on bi-stable flows of a notchback bluff body,” *Phys. Fluids*, vol. 33, no. 12, p. 125113, 2021, doi: 10.1063/5.0080125.

[10] K. He, G. Minelli, X. Su, J. Wang, G. Gao, and S. Krajnović, “Floor motion’s influence on wake asymmetry of a notchback bluff body,” *Phys. Fluids*, vol. 34, no. 3, p. 035128, 2022, doi: 10.1063/5.0084435.

[11] N. F. Ouedraogo and E. E. Essel, “Effects of Reynolds number on the wake characteristics of a notchback Ahmed body,” *J. Fluids Eng.*, vol. 146, no. 1, pp. 011303-1–011303-13, 2024, doi: 10.1115/1.4065225.

[12] M. Samimy and S. K. Lele, “Motion of particles with inertia in a compressible free shear layer,” *Phys. Fluids A*, vol. 3, no. 8, pp. 1915–1923, 1991, doi: 10.1063/1.857926.

[13] B. R. Munson, T. H. Okiishi, W. W. Huebsch, and A. P. Rothmayer, *Fluid Mechanics*, 7th ed. Hoboken, NJ, USA: Wiley, 2013, pp. 271–274.

[14] L. Sirovich, “Turbulence and the dynamics of coherent structures. I. Coherent structures,” *Q. Appl. Math.*, vol. 45, no. 3, pp. 561–571, 1987, doi: 10.1090/qam/910462.

[15] A. Towne, O. T. Schmidt, and T. Colonius, "Spectral proper orthogonal decomposition and its relationship to dynamic mode decomposition and resolvent analysis," *J. Fluid Mech.*, vol. 847, pp. 821–867, 2018, doi: 10.1017/jfm.2018.283.

[16] E. E. Essel, R. Balachandar, and M. F. Tachie, "Effects of sheltering on the unsteady wake dynamics of tandem cylinders mounted in a turbulent boundary layer," *J. Fluid Mech.*, vol. 954, p. A40, 2023, doi: 10.1017/jfm.2023.122.